Andreev bound states and the π-junction transition in a superconductor/quantum-dot/superconductor system

2001 J. Phys.: Condens. Matter 13 8783

(http://iopscience.iop.org/0953-8984/13/39/307)

INSTITUTE OF PHYSICS PUBLISHING JOURNAL OF PHYSICS: CONDENSED MATTER

J. Phys.: Condens. Matter **13** (2001) 8783–8798 PII: S0953-8984(01)23245-7

Andreev bound states and the π-junction transition in a superconductor/quantum-dot/superconductor system

Yu Zhu, Qing-feng Sun and Tsung-han Lin[1]

State Key Laboratory for Mesoscopic Physics and Department of Physics, Peking University, Beijing 100871, China

Received 22 March 2001, in final form 23 July 2001
Published 13 September 2001
Online at stacks.iop.org/JPhysCM/13/8783

Abstract

We study Andreev bound states and the π-junction transition in a superconductor/quantum-dot/superconductor (S–QD–S) system by a Green function method. We derive an equation for describing the Andreev bound states in the S–QD–S system, and provide a unified understanding of the π-junction transition caused by three different mechanisms. (1) *Zeeman splitting*. For a QD with two spin levels $E_\uparrow$ and $E_\downarrow$, we find that the surface of the Josephson current $I(\phi = \pi/2)$ versus the $(E_\uparrow, E_\downarrow)$ configuration exhibits an interesting profile: a sharp peak around $E_\uparrow = E_\downarrow = 0$; a positive ridge in the region of $E_\uparrow E_\downarrow > 0$; and a *negative*, flat, shallow plane in the region of $E_\uparrow E_\downarrow < 0$. (2) *Intra-dot interaction*. We deal with the intra-dot Coulomb interaction by using the Hartree–Fock approximation, and find that the system behaves as a π-junction when the QD becomes a magnetic dot due to the interaction. The conditions for π-junction transition are also discussed. (3) *Non-equilibrium distribution*. We replace the Fermi distribution, $f(\omega)$, by a non-equilibrium one, $\frac{1}{2}[f(\omega - V_c) + f(\omega + V_c)]$, and allow Zeeman splitting in the QD where $E_\uparrow = -E_\downarrow = h$. The curves of $I(\phi = \pi/2)$ versus V_c show the novel effect of the interplay of the non-equilibrium distribution with magnetization in the QD.

1. Introduction

Superconductivity has the nature of quantum condensation on a macroscopic scale, which can be described by a wavefunction with phase factor $e^{i\phi}$. When two superconductors are weakly linked, the phase difference will manifest itself in the dc Josephson current, with the current–phase relation $I = I_c \sin(\phi_1 - \phi_2)$. If the weak-link area is controlled by certain external conditions, the magnitude of the critical current I_c may be either suppressed [1] or enhanced [2]. On some occasions, even the sign of I_c may be reversed [3], or equivalently the

[1] Author to whom any correspondence should be addressed.

phase factor $\sin(\phi_1 - \phi_2)$ may change to $\sin(\phi_1 - \phi_2 + \pi)$; this is referred to as the π-junction transition. One of the simplest examples is so-called superconducting quantum diffraction, in which a superconductor/insulator/superconductor tunnel junction is tuned by an external magnetic field. The dc Josephson current versus the magnetic flux Φ_B has the form

$$I = I_c \left[\frac{\sin \pi \Phi_B / \Phi_0}{\pi \Phi_B / \Phi_0} \right] \sin(\phi_1 - \phi_2)$$

and changes sign every time Φ_B / Φ_0 is equal to an integer. Unfortunately, the π-junction transition cannot be directly detected in the two-terminal tunnel junction because the current source is used in the measurement to control the supercurrent rather than the phase difference. However, in a mesoscopic superconductor/normal-metal/superconductor (SNS) junction with the N-region coupled to normal electrode(s) [4, 5], the phase difference can be determined independently from the coherent Andreev reflection current which is proportional to

$$|e^{i\phi_1} + e^{i\phi_2}|^2 = 2[1 + \cos(\phi_1 - \phi_2)].$$

Thus, direct observation of the π-junction transition becomes possible.

In mesoscopic SNS junctions, supercurrent is conducted through the N-region by the Andreev reflection (AR) process [6]. The energy gaps of two superconducting electrodes serve as two 'mirrors', reflecting an electron into a hole and a hole into an electron. For ballistic SNS junctions, discrete Andreev bound states are formed in the N-region; each state carries positive or negative supercurrent. For diffusive SNS junctions, the so-called current-carrying density of states (CCDOS) plays a similar role, and also makes positive and negative contributions to the supercurrent. A recent experiment [3] demonstrated the π-junction transition in the diffusive SNS junction by applying a control voltage to the N-region. In fact, biased normal reservoirs across a mesoscopic N-region induce a non-equilibrium distribution in the N-region, and make the occupied fraction of the CCDOS deviate from the equilibrium one. When the control voltage exceeds a certain value, the non-equilibrium distribution has so much weight in the negative part of the CCDOS that the total current reverses its sign. Many theoretical works have addressed this issue, either for ballistic SNS junctions [7–11], or for diffusive SNS junctions [12–15].

In addition to non-equilibrium distribution, there is a completely different mechanism for realizing the π-junction transition, i.e., coupling superconductors by an Anderson impurity or an interacting quantum dot (QD). The works of Glazman and Matveev [16] and Spivak and Kivelson [17] revealed that when the impurity is singly occupied, the sign of the Josephson current for infinite Coulomb repulsion is opposite to that without the repulsion. Ishizaka *et al* [18] obtained the condition for π-junction transition, by using the non-crossing approximation and varying the strength of the Coulomb repulsion, the bare-level position, the tunnelling strength, and the temperature. Rozhkov and Arovas [19] analysed the system in a non-perturbative way, and found a novel intermediate phase in which one of $\phi = 0$ and $\phi = \pi$ is stable while the other is metastable, with the energy $E(\phi)$ having a kink somewhere in between. Clerk and Ambegaokar [20] studied the case of infinite U and the regime where the superconducting gap Δ and the Kondo temperature T_K are comparable, and showed that the position of the sub-gap resonance in the impurity spectral function develops a strong anomalous phase dependence, and the π-junction behaviour is lost as the position of the bound state moves above the Fermi energy.

Recently, there has been growing interest in the physics of a superconductor in contact with ferromagnetic material, and the following works revealed another approach to achieving the π-junction. Prokić *et al* [21] presented a theory of the π-junction transition in atomic-scale superconductor/ferromagnet (S/F) superlattices. They found that the critical Josephson current has a non-monotonic dependence on the exchange field h in the ferromagnetic layer,

becoming zero at the critical value corresponding to the transition between $\phi = 0$ and $\phi = \pi$ in the ground state. Yip [22] and Heikkilä *et al* [23] demonstrated that the supercurrent through a mesoscopic SFS junction oscillates with an exponentially decreasing envelope as a function of the exchange field or the distance between the electrodes. They also proposed that the supercurrent suppressed by the exchange field can be recovered by an appropriate non-equilibrium distribution.

With these facts in mind, we are curious as to whether there is any relationship among the above three mechanisms for achieving π-junction transition. Motivated by this, we investigate the following cases of π-junction transition in a superconductor/quantum-dot/superconductor (S–QD–S) system and provide a unified picture based on Andreev bound states. In section 2, we study the π-junction transition caused by Zeeman splitting. Assuming the QD to have two spin levels, $E_\uparrow$ and $E_\downarrow$, we find that the surface of the Josephson current $I(\pi/2)$ versus the $(E_\uparrow, E_\downarrow)$ configuration exhibits an interesting profile: a sharp peak around $E_\uparrow = E_\downarrow = 0$; a positive ridge in the region of $E_\uparrow E_\downarrow > 0$; and a *negative*, flat, shallow plane in the region of $E_\uparrow E_\downarrow < 0$. In section 3, we study the π-junction transition caused by intra-dot interaction. We model QD by

$$H_{dot} = E_0 \sum_\sigma c_\sigma^\dagger c_\sigma + U n_\uparrow n_\downarrow$$

and handle the interaction term by using the Hartree–Fock approximation. Thus this case is reduced to the first one except for a self-consistent calculation for $\langle n_\sigma \rangle$. We show that the π-junction transition occurs when the QD becomes a magnetic dot due to the interaction. The conditions for π-junction transition are also discussed. In section 4, we study the π-junction transition caused by non-equilibrium distribution in the QD. By replacing the Fermi distribution, $f(\omega)$, with a non-equilibrium one, $\frac{1}{2}[f(\omega - V_c) + f(\omega + V_c)]$, and allowing Zeeman splitting in the QD: $E_\uparrow = -E_\downarrow = h$, we find that for $h = 0$, the supercurrent reverses its sign when the control voltage V_c exceeds a certain value, which is in agreement with previous work [24] and the experiment in [3]. For $h \neq 0$, the curves of Josephson current versus control voltage show a novel effect of interplay of the non-equilibrium distribution with the magnetization in the QD. Finally, we summarize our understanding of π-junction transition in the S–QD–S system in section 5.

2. QD with two spin levels

2.1. The model Hamiltonian and formulation

In this section, we study the S–QD–S system modelled by the following Hamiltonian:

$$H = H_L + H_R + H_{dot} + H_T \tag{1}$$

where

$$H_L = \sum_{k\sigma} \epsilon_k a_{k\sigma}^\dagger a_{k\sigma} + \sum_k \left[\Delta e^{-i\phi_L} a_{k\uparrow}^\dagger a_{-k\downarrow}^\dagger + \text{h.c.} \right]$$

$$H_R = \sum_{p\sigma} \epsilon_p b_{p\sigma}^\dagger b_{p\sigma} + \sum_p \left[\Delta e^{-i\phi_R} b_{p\uparrow}^\dagger b_{-p\downarrow}^\dagger + \text{h.c.} \right]$$

$$H_{dot} = \sum_\sigma E_\sigma c_\sigma^\dagger c_\sigma$$

$$H_T = \sum_{k\sigma} \left[t_L a_{k\sigma}^\dagger c_\sigma + \text{h.c.} \right] + \sum_{p\sigma} \left[t_R b_{p\sigma}^\dagger c_\sigma + \text{h.c.} \right]$$

where H_L and H_R describe the left and right superconducting leads with phase difference[2] $\phi_L - \phi_R$, H_{dot} describes the quantum dot with two spin levels, and H_T is the coupling between the quantum dot and the superconducting leads.

Since the Josephson current can be expressed in terms of the Green functions of the QD, we first derive the Green function by solving the Dyson equation. Following the formulation in [25], we denote by $\mathbf{G}$ and $\mathbf{g}$ the Green functions of the QD in the Nambu representation, with and without the coupling to the leads, respectively; and denote by $\mathbf{\Sigma}$ the self-energy due to the coupling between the QD and the leads. The retarded Green function (Fourier transformed) of the isolated QD is

$$\mathbf{g}^r = \begin{pmatrix} \dfrac{1}{\omega - E_\uparrow + \mathrm{i}0^+} & 0 \\ 0 & \dfrac{1}{\omega + E_\downarrow + \mathrm{i}0^+} \end{pmatrix}. \tag{2}$$

The retarded self-energy (Fourier transformed) under the wide-bandwidth approximation can be derived as [25]

$$\mathbf{\Sigma}^r_{L/R}(\omega) = -\frac{\mathrm{i}}{2}\Gamma_{L/R}\rho(\omega) \begin{pmatrix} 1 & -\dfrac{\Delta}{\omega}\mathrm{e}^{-\mathrm{i}\phi_{L/R}} \\ -\dfrac{\Delta}{\omega}\mathrm{e}^{\mathrm{i}\phi_{L/R}} & 1 \end{pmatrix} \tag{3}$$

where $\Gamma_{L/R}$ is the strength of the coupling between the superconducting leads and the QD, defined by $\Gamma_{L/R} \equiv 2\pi N_{L/R} t^2_{L/R}$, in which N_L and N_R are the densities of states in the left and right leads in the normal state. The factor $\rho(\omega)$ is defined as

$$\rho(\omega) \equiv \begin{cases} \dfrac{|\omega|}{\sqrt{\omega^2 - \Delta^2}} & |\omega| > \Delta \\ \dfrac{\omega}{\mathrm{i}\sqrt{\Delta^2 - \omega^2}} & |\omega| < \Delta. \end{cases} \tag{4}$$

Notice that $\rho(\omega)$ is the ordinary dimensionless BCS density of states when $|\omega| > \Delta$, but has an imaginary part when $|\omega| < \Delta$, corresponding to the Andreev reflection process within the superconducting gap. For simplicity, we assume that the two superconducting leads are identical except for a phase difference. Let $\phi_L = \phi/2$, $\phi_R = -\phi/2$, $\Gamma_L = \Gamma_R \equiv \Gamma$; then we obtain

$$\mathbf{\Sigma}^r \equiv \mathbf{\Sigma}^r_L + \mathbf{\Sigma}^r_R = -\mathrm{i}\Gamma\rho(\omega) \begin{pmatrix} 1 & -\dfrac{\Delta}{\omega}\cos\dfrac{\phi}{2} \\ -\dfrac{\Delta}{\omega}\cos\dfrac{\phi}{2} & 1 \end{pmatrix} \tag{5}$$

$$\tilde{\mathbf{\Sigma}}^r \equiv \mathbf{\Sigma}^r_L - \mathbf{\Sigma}^r_R = -\mathrm{i}\Gamma\rho(\omega) \begin{pmatrix} 0 & -\dfrac{\Delta}{\omega}(-\mathrm{i})\sin\dfrac{\phi}{2} \\ -\dfrac{\Delta}{\omega}\mathrm{i}\,\sin\dfrac{\phi}{2} & 0 \end{pmatrix}. \tag{6}$$

By using the Dyson equation, the retarded Green function of QD can be obtained as

$$\mathbf{G}^r = \left[\mathbf{g}^{r^{-1}} - \mathbf{\Sigma}^r\right]^{-1} = \frac{1}{A}\begin{pmatrix} g^{r^{-1}}_{22} - \Sigma^r_{22} & \Sigma^r_{12} \\ \Sigma^r_{21} & g^{r^{-1}}_{11} - \Sigma^r_{11} \end{pmatrix} \tag{7}$$

where $A = A(\omega)$ is defined as

$$A(\omega) \equiv \det[\mathbf{g}^{r^{-1}} - \mathbf{\Sigma}^r] = (g^{r^{-1}}_{22} - \Sigma^r_{22})(g^{r^{-1}}_{11} - \Sigma^r_{11}) - \Sigma^r_{12}\Sigma^r_{21}. \tag{8}$$

[2] The phase factor is $\mathrm{e}^{-\mathrm{i}\phi}$ instead of $\mathrm{e}^{\mathrm{i}\phi}$, since we choose $e = 1$ instead of $e = -1$.

The general current formula for a mesoscopic hybrid multi-terminal system has been derived in [25]. For the time-independent case and the QD with two spin levels under consideration, the current formula can be rewritten in a compact form (in units of $e = \hbar = 1$):

$$I_{L/R} = I_{L/R,\uparrow} + I_{L/R,\downarrow} = \int \frac{\mathrm{d}\omega}{2\pi}\, 2\,\mathrm{Re}[\mathbf{G}\mathbf{\Sigma}_{L/R}]^{<}_{11-22} \tag{9}$$

where $[CD]^{<} \equiv C^{<}D^{a} + C^{r}D^{<}$, $[\ ]_{11-22} \equiv [\ ]_{11} - [\ ]_{22}$, and $\mathbf{G}$, $\mathbf{\Sigma}_{L/R}$ are the Fourier transformed 2×2 Nambu matrices. Since $I = I_L = -I_R$ in the stationary transport, the current formula can be further reduced to

$$I = \frac{1}{2}(I_L - I_R) = \int \frac{\mathrm{d}\omega}{2\pi}\ \mathrm{Re}[\mathbf{G}\tilde{\mathbf{\Sigma}}]^{<}_{11-22} \tag{10}$$

with $\tilde{\mathbf{\Sigma}} \equiv \mathbf{\Sigma}_L - \mathbf{\Sigma}_R$. Applying the fluctuation-dissipation theorem, one has

$$\mathbf{G}^{<} = f(\omega)[\mathbf{G}^{a} - \mathbf{G}^{r}] \qquad \tilde{\mathbf{\Sigma}}^{<} = f(\omega)[\tilde{\mathbf{\Sigma}}^{a} - \tilde{\mathbf{\Sigma}}^{r}]$$

where $f(\omega) = 1/(\mathrm{e}^{\beta\omega} + 1)$ is the Fermi distribution function. Notice that $(\mathbf{G}^{r})^{\dagger} = \mathbf{G}^{a}$, $(\tilde{\mathbf{\Sigma}}^{r})^{\dagger} = \tilde{\mathbf{\Sigma}}^{a}$; the expression in the integrand can be simplified to

$$\mathrm{Re}[\mathbf{G}\tilde{\mathbf{\Sigma}}]^{<}_{11-22} = f(\omega)\, 2\sin\phi \frac{\Gamma^2\Delta^2}{\omega^2 - \Delta^2}\left[-\,\mathrm{Im}\,\frac{1}{A(\omega)}\right]. \tag{11}$$

Consequently, the Josephson current is expressed as

$$I = 2\sin\phi \int \frac{\mathrm{d}\omega}{2\pi}\ f(\omega)\, j(\omega) \tag{12}$$

in which the current-carrying density of states (CCDOS) $j(\omega)$ is defined by

$$j(\omega) \equiv \frac{\Gamma^2\Delta^2}{\omega^2 - \Delta^2}\left[-\,\mathrm{Im}\,\frac{1}{A(\omega)}\right]. \tag{13}$$

Because the singularities of $j(\omega)$ lie in the same half-plane, the CCDOS $j(\omega)$ satisfies the condition

$$\int j(\omega)\ \mathrm{d}\omega = 0.$$

Since $\Sigma^{r}(\omega)$ is purely imaginary when $|\omega| > \Delta$ while it is purely real when $|\omega| < \Delta$, $A(\omega)$ has a finite imaginary part when $|\omega| > \Delta$, while it has an infinitesimal imaginary part when $|\omega| < \Delta$. Correspondingly, the Josephson current can be divided into two parts, contributed by the continuous spectrum and the discrete spectrum:

$$\begin{aligned} I &= I_c + I_d \\ I_c &\equiv 2\sin\phi\left(\int_{-\infty}^{-\Delta} + \int_{\Delta}^{\infty}\right)\frac{\mathrm{d}\omega}{2\pi}\ f(\omega)\, j(\omega) \\ I_d &\equiv 2\sin\phi \int_{-\Delta}^{\Delta} \frac{\mathrm{d}\omega}{2\pi}\ f(\omega)\, j(\omega). \end{aligned} \tag{14}$$

We shall show in the appendix that when $|\omega| < \Delta$ and $\phi \neq 0$, the equation $A(\omega) = 0$ has two real roots denoted by $\tilde{E}_1 = \Delta\sin\theta_1$ and $\tilde{E}_2 = \Delta\sin\theta_2$, where θ_1 and θ_2 are the two roots of the following equation:

$$\left(\sin\theta + \frac{\Gamma}{\Delta}\tan\theta - \frac{E_{\uparrow}}{\Delta}\right)\left(\sin\theta + \frac{\Gamma}{\Delta}\tan\theta + \frac{E_{\downarrow}}{\Delta}\right)\cos^2\theta - \frac{\Gamma^2}{\Delta^2}\cos^2\frac{\phi}{2} = 0 \tag{15}$$

with $\theta \in (-\pi/2, \pi/2)$. Equation (15) completely determines the properties of Andreev bound states. The roots $\tilde{E}_1$ and $\tilde{E}_2$ are just the Andreev bound states. In the range $|\omega| < \Delta$, $A(\omega)$ can be written as $a(\omega)(\omega - \tilde{E}_1 + \mathrm{i}0^+)(\omega - \tilde{E}_2 + \mathrm{i}0^+)$, and $[-\operatorname{Im}\{1/A(\omega)\}]$ is reduced to

$$-\operatorname{Im}\frac{1}{A(\omega)} = \pi\left[\frac{1}{A'(\tilde{E}_1)}\delta(\omega - \tilde{E}_1) + \frac{1}{A'(\tilde{E}_2)}\delta(\omega - \tilde{E}_2)\right]. \tag{16}$$

Finally, the Josephson current through the S–QD–S system can be expressed as

$$\begin{aligned} I &= I_c + I_d \\ I_c &\equiv 2\sin\phi\left(\int_{-\infty}^{-\Delta} + \int_{\Delta}^{\infty}\right)\frac{\mathrm{d}\omega}{2\pi}\, f(\omega)\frac{\Gamma^2\Delta^2}{\omega^2 - \Delta^2}\left[-\operatorname{Im}\frac{1}{A(\omega)}\right] \\ I_d &\equiv \sin\phi\left[f(\tilde{E}_1)\frac{\Gamma^2\Delta^2}{\tilde{E}_1^2 - \Delta^2}\frac{1}{A'(\tilde{E}_1)} + f(\tilde{E}_2)\frac{\Gamma^2\Delta^2}{\tilde{E}_2^2 - \Delta^2}\frac{1}{A'(\tilde{E}_2)}\right]. \end{aligned} \tag{17}$$

This current formula will be used in the following numerical study[3].

2.2. Numerical results and discussion

Now we discuss the numerical results for Andreev bound states and the Josephson current. In all of the numerical studies of this paper, we take $e = \hbar = k_B = 1$, set $\Delta = 1$, i.e., measure all energies in units of Δ, let $\Gamma = 0.1$ for the symmetric and weak-coupling case, and fix the phase difference $\phi = \pi/2$.

Figure 1 presents the solution of equation (15), i.e., Andreev bound states of the S–QD–S system. In the limit $\Gamma \to \infty$, equation (15) gives

$$\tilde{E}_1 = |\cos(\phi/2)| \qquad \tilde{E}_2 = -|\cos(\phi/2)|.$$

These are the well-known Andreev bound states for a clean superconducting point contact [26–28]. Conversely, in the limit $\Gamma \to 0$, the two roots of equation (15) are $\tilde{E}_1 = E_\uparrow$ and $\tilde{E}_1 = -E_\downarrow$, i.e., the bare levels of the electron with spin $\uparrow$ and hole with spin $\downarrow$ of the QD. (We describe spin-$\uparrow$ quasiparticles in electron language and spin-$\downarrow$ quasiparticles in hole language due to the choice of the Nambu representation.) For the case of $\Gamma \ll \Delta$ under consideration, where the QD is weakly coupled with the superconducting leads, the solutions of equation (15) depend strongly on the configuration of the QD levels $(E_\uparrow, E_\downarrow)$, but weakly on the phase difference ϕ. The surfaces of $\tilde{E}_1$ versus $(E_\uparrow, E_\downarrow)$ and $\tilde{E}_2$ versus $(E_\uparrow, E_\downarrow)$ for $\phi = \pi/2$ are shown in figure 1(a) and figure 1(b), respectively. In this case, the electron level $E_\uparrow$ and the hole level $-E_\downarrow$ are coupled by AR tunnelling. Therefore, Andreev bound states can be viewed as hybrids of $E_\uparrow$ and $-E_\downarrow$, and an energy gap of the order of Γ is opened where $E_\uparrow$ and $-E_\downarrow$ are equal (see figure 1(c) and figure 1(d)). Further study on the relations of $\tilde{E}_1$ versus ϕ and $\tilde{E}_2$ versus ϕ can provide the supercurrent carried by each Andreev bound state (not shown).

Figure 2 presents the surface of the Josephson current I versus the $(E_\uparrow, E_\downarrow)$ configuration. First, the surface is symmetric with respect to the diagonal lines $E_\uparrow = E_\downarrow$ and $E_\uparrow = -E_\downarrow$, which reflects the symmetry of the electron and hole and the fact that the supercurrents are non-spin-polarized. Second, the surface exhibits an interesting profile: a sharp peak around $E_\uparrow = E_\downarrow = 0$; a positive ridge in the region of $E_\uparrow E_\downarrow > 0$; and a negative, flat, shallow plane in the region of $E_\uparrow E_\downarrow < 0$. Note that the positive ridge and negative plane share a sharp edge. Third, consider two special but typical cases, $E_\uparrow = E_\downarrow \equiv E_0$ (figure 2(b)) and $E_\uparrow = -E_\downarrow \equiv E_0$ (figure 2(c)), which are actually the diagonal cuts of figure 2(a). For the case

[3] The contribution from the discrete spectrum can also be derived from the dispersion relation for Andreev bound states, $I_d = 2[(\partial\tilde{E}_1/\partial\phi)f(\tilde{E}_1) + (\partial\tilde{E}_2/\partial\phi)f(\tilde{E}_2)]$.

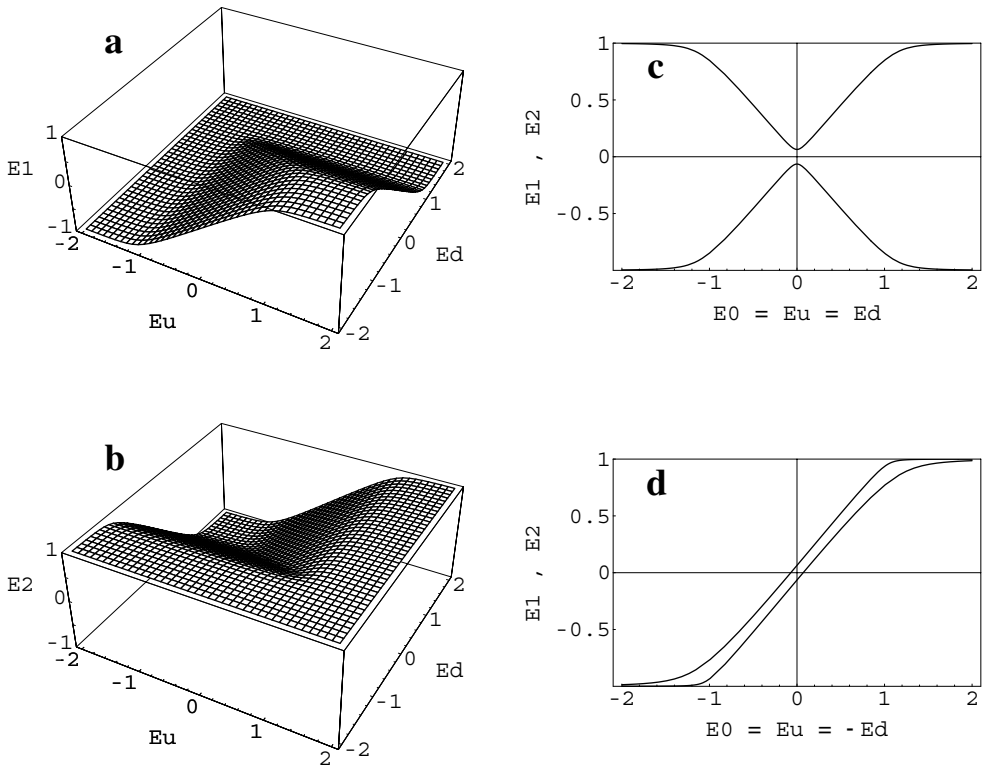

Figure 1. Solution of the equation for Andreev bound states. The parameters are: $\Delta = 1, \Gamma = 0.1, \phi = \pi/2$. (a) and (b) show the two roots $\tilde{E}_1$ and $\tilde{E}_2$ ($\tilde{E}_1 > \tilde{E}_2$) versus the configurations of QD levels ($E_\uparrow$, $E_\downarrow$). (c) and (d) display the diagonal cuts of (a) and (b), showing $\tilde{E}_1$ and $\tilde{E}_2$ versus E_0 with $E_\uparrow = E_\downarrow \equiv E_0$ and $E_\uparrow = -E_\downarrow \equiv E_0$, respectively. $\tilde{E}_1$ and $\tilde{E}_2$ can be viewed as two hybrid levels of the electron level of $E = E_\uparrow$ and the hole level of $E = -E_\downarrow$. ($\tilde{E}_1$, $\tilde{E}_2$, $E_\uparrow$, and $E_\downarrow$ are marked as E1, E2, Eu, and Ed in the plots, respectively.)

of $E_\uparrow = E_\downarrow$, the I versus E_0 curve has a peak at $E_0 = 0$ with a width of Γ, which reproduces the result for the QD with one spin-degenerate level [24]. For the case of $E_\uparrow = -E_\downarrow$, the I versus E_0 curve has the same maximum at $E_0 = 0$, but jumps suddenly from the positive maximum to a small negative value around $E_0 = \pm\Gamma$, which is quite similar to the case for the curve of the critical current versus the exchange field for an atomic-scale S/F superlattice (see figure 2 of [21]).

To understand these features, we plot the CCDOS $j(\omega)$ for different configurations of ($E_\uparrow$, $E_\downarrow$) in figure 3. The supercurrent can be expressed as

$$I = 2\sin\phi \int \frac{\mathrm{d}\omega}{2\pi}\, f(\omega) j(\omega)$$

and only the spectrum of $\omega < 0$ relates to the current at zero temperature. For the spectrum of $E_\uparrow = E_\downarrow = 0$, $j(\omega)$ has two δ-function-type discrete spectra within the superconducting gap, corresponding to two Andreev bound states. They carry supercurrents with opposite signs: positive for $\tilde{E}_1 < 0$ and negative for $\tilde{E}_2 > 0$. $j(\omega)$ also has a continuous spectrum outside the superconducting gap, negative and positive for $\omega < -\Delta$ and $\omega > \Delta$, respectively. Since the contribution from the discrete spectrum is much larger than that from the continuous one, the current peak at $E_\uparrow = E_\downarrow = 0$ is mostly contributed by $\tilde{E}_1$. For the spectrum of

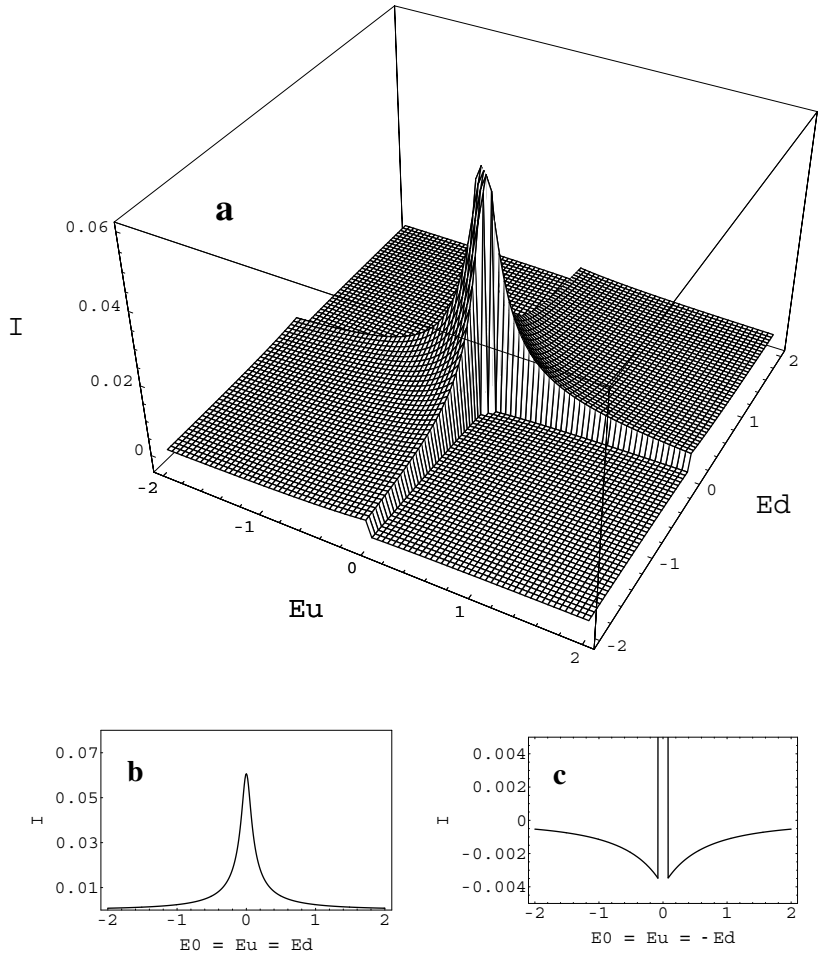

Figure 2. The surface of the Josephson current I versus the configuration of the QD levels $(E_\uparrow, E_\downarrow)$. The parameters are: $\Delta = 1, \Gamma = 0.1, \phi = \pi/2, T = 0$. (a) is the surface graph, while (b), (c) display the diagonal cuts. (b) and (c) show I versus E_0 with $E_\uparrow = E_\downarrow \equiv E_0$ and $E_\uparrow = -E_\downarrow \equiv E_0$, respectively.

$E_\uparrow = E_\downarrow = E_0 \neq 0$, $\tilde{E}_1$ and $\tilde{E}_2$ move toward $\pm\Delta$, symmetrically with respect to the Fermi surface (see also figure 1(c)). The contribution from the discrete spectrum $\tilde{E}_1$ decreases continuously with E_0, corresponding to the Γ-width broadening of the $E_0 = 0$ peak in figure 2(c). For the spectrum of $E_\uparrow = -E_\downarrow = E_0 \neq 0$, however, $\tilde{E}_1$ and $\tilde{E}_2$ move in the same direction. When $E_0 < -\Gamma$ or $E_0 > \Gamma$, both $\tilde{E}_1$ and $\tilde{E}_2$ are below or above the Fermi surface (see also figure 1(d)). As a consequence, they make little net contribution to the supercurrent, and the relatively small negative continuous spectrum of $\omega < -\Delta$ dominates. Because the crossover of $\tilde{E}_1$ and $\tilde{E}_2$ from different sides of the Fermi surface to one side occurs abruptly, sudden jumps between the positive maximum and the negative valleys appear in figure 2(d). Similarly, one can understand the whole surface of figure 2 with the help of the Andreev bound states in figure 1 and the properties of the CCDOS in figure 3.

The above results are for zero temperature; the temperature dependence of the Josephson current is shown in figure 4. Notice that the supercurrent is sensitive to the temperature. The

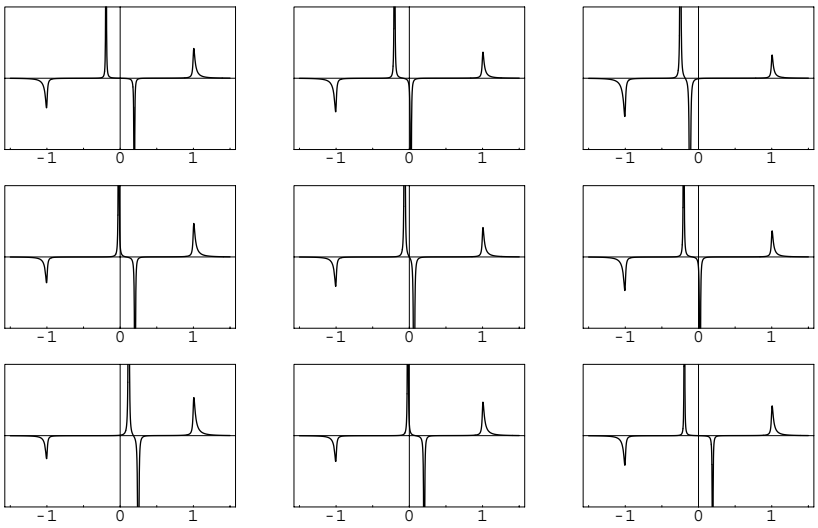

Figure 3. CCDOS $j(\omega)$ for different $(E_\uparrow, E_\downarrow)$ configurations. The rows from top to bottom correspond to $E_\uparrow = -0.2, 0, 0.2$, and the columns from left to right correspond to $E_\downarrow = -0.2, 0, 0.2$. Each of the CCDOS contains two types of spectrum: the discrete spectrum in the range $|\omega| < 1$ and the continuous spectrum in the range $|\omega| > 1$. To illustrate the discrete spectrum, we broaden the δ-functions by 0.01 in the plots.

height of the $E_\uparrow = E_\downarrow = 0$ peak (referred to as I_0) decreases rapidly with the increase of the temperature, $I_0 = 0.06, 0.004, 0.001$ for $T = 0, 0.25, 0.50$, respectively. The sharp edge between $I > 0$ and $I < 0$ is also smeared out at finite temperatures. The reason for this is that at finite temperature not only the Andreev bound state below the Fermi surface but also the one above the Fermi surface makes a contribution to the supercurrent.

3. QD with intra-dot interaction

3.1. Hartree–Fock approximation

In this section, we investigate the π-junction transition caused by the intra-dot interaction. The quantum dot with Coulomb interaction can be described by

$$H_{dot} = E_0 \sum_\sigma c_\sigma^\dagger c_\sigma + U n_\uparrow n_\downarrow.$$

As in the problem of the local moment in non-magnetic metals [29], we deal with the interaction term by using the Hartree–Fock approximation (HFA), in which $U n_\uparrow n_\downarrow$ is replaced by $U\langle n_\uparrow\rangle n_\downarrow + U n_\uparrow \langle n_\downarrow\rangle$. Thus, H_{dot} becomes

$$H_{dot} = \sum_\sigma E'_\sigma c_\sigma^\dagger c_\sigma$$

with the effective levels $E'_\sigma \equiv E_0 + U\langle n_{\bar\sigma}\rangle$. Despite the roughness of the HFA, it contains the physics of the magnetization due to the Coulomb interaction. More important, the approximation allows us to obtain a solution including infinite orders of tunnelling processes, which is crucial for describing the Andreev bound states and the supercurrent that they carry. However, the HFA fails in the Kondo regime. As discussed in [20], if

$$\Delta \ll T_K \equiv \sqrt{\{U\Gamma\}} \mathrm{e}^{-\pi|E_0-\mu|/\Gamma}$$

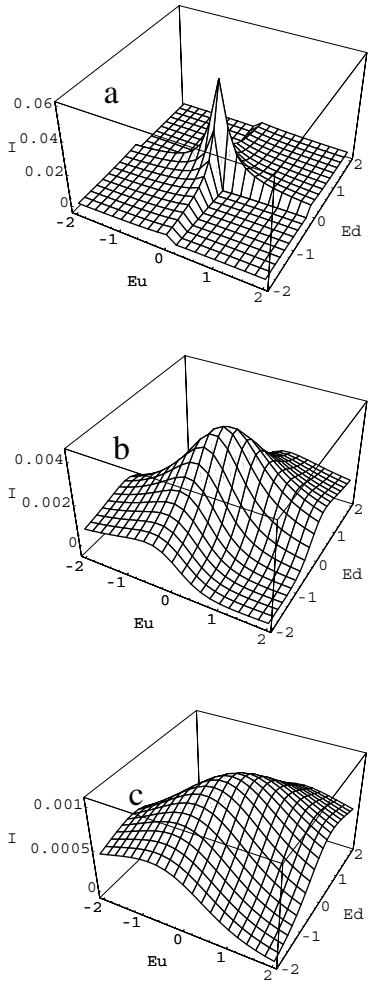

Figure 4. Surfaces of Josephson current I versus $(E_\uparrow, E_\downarrow)$ configurations at different temperatures: $T = 10^{-4}$, 0.25, 0.50 for (a), (b), and (c), respectively. The other parameters are the same as for figure 1.

the spin of the impurity is completely screened by Kondo effect, and there will be no π-junction behaviour. In this work, we will restrict consideration to the weak-coupling case where the magnetization effect dominates, corresponding to the $\Delta \gg T_K$ regime.

Then most of the formulae in the previous section can be carried over, except that for the averaged occupation number $\langle n_\sigma \rangle$, which needs a self-consistent calculation. Notice that $\langle n_\sigma \rangle$ can be derived from the retarded Green function of QD as

$$\langle n_\uparrow \rangle = \int \frac{\mathrm{d}\omega}{2\pi} f(\omega) \left[-2 \operatorname{Im} G^r_{11}(\omega) \right] \tag{18}$$

$$1 - \langle n_\downarrow \rangle = \int \frac{\mathrm{d}\omega}{2\pi} f(\omega) \left[-2 \operatorname{Im} G^r_{22}(\omega) \right]. \tag{19}$$

Like the current, $\langle n_\sigma \rangle$ can be divided into two parts, the contribution from the discrete spectrum

and the contribution from the continuous spectrum:

$$\begin{aligned}
\langle n_\uparrow \rangle &= \langle n_\uparrow \rangle_c + \langle n_\uparrow \rangle_d \\
\langle n_\uparrow \rangle_c &= \left(\int_{-\infty}^{-\Delta} + \int_{\Delta}^{\infty} \right) \frac{\mathrm{d}\omega}{2\pi} \, f(\omega) \left[-2 \,\mathrm{Im} \, \frac{g_{22}^{r^{-1}}(\omega) - \Sigma_{22}^{r}(\omega)}{A(\omega)} \right] \\
\langle n_\uparrow \rangle_d &= \sum_{i=1}^{2} \left[f(\omega) \frac{1}{A'(\omega)} (g_{22}^{r^{-1}}(\omega) - \Sigma_{22}^{r}(\omega)) \right]_{\omega = \tilde{E}_i}
\end{aligned} \tag{20}$$

and

$$\begin{aligned}
\langle n_\downarrow \rangle &= \langle n_\downarrow \rangle_c + \langle n_\downarrow \rangle_d \\
1 - \langle n_\downarrow \rangle_c &= \left(\int_{-\infty}^{-\Delta} + \int_{\Delta}^{\infty} \right) \frac{\mathrm{d}\omega}{2\pi} \, f(\omega) \left[-2 \,\mathrm{Im} \, \frac{g_{11}^{r^{-1}}(\omega) - \Sigma_{11}^{r}(\omega)}{A(\omega)} \right] \\
1 - \langle n_\downarrow \rangle_d &= \sum_{i=1}^{2} \left[f(\omega) \frac{1}{A'(\omega)} (g_{11}^{r^{-1}}(\omega) - \Sigma_{11}^{r}(\omega)) \right]_{\omega = \tilde{E}_i} .
\end{aligned} \tag{21}$$

Since $\mathbf{g}^r$ contains the unknown quantity $\langle n_\sigma \rangle$ through E'_σ, the above equations for $\langle n_\sigma \rangle$ should be solved self-consistently.

3.2. Numerical results and discussion

Next, we present the numerical results for the interacting QD system at zero temperature. Figure 5 shows I versus E_0 and the corresponding $\langle n_\sigma \rangle$ versus E_0 curves for two typical cases, the QD without interaction ($U = 0$, in figure 5(a)) and with strong interaction ($U \gg \Gamma$, in figure 5(b)). The S–QD–S system behaves like one of the above two cases, Depending on the magnitudes of the interacting constant U and the coupling strength Γ, the S–QD–S system may behave differently. If $U < \Gamma$, the occupation numbers $\langle n_\uparrow \rangle$ and $\langle n_\downarrow \rangle$ are almost equal,

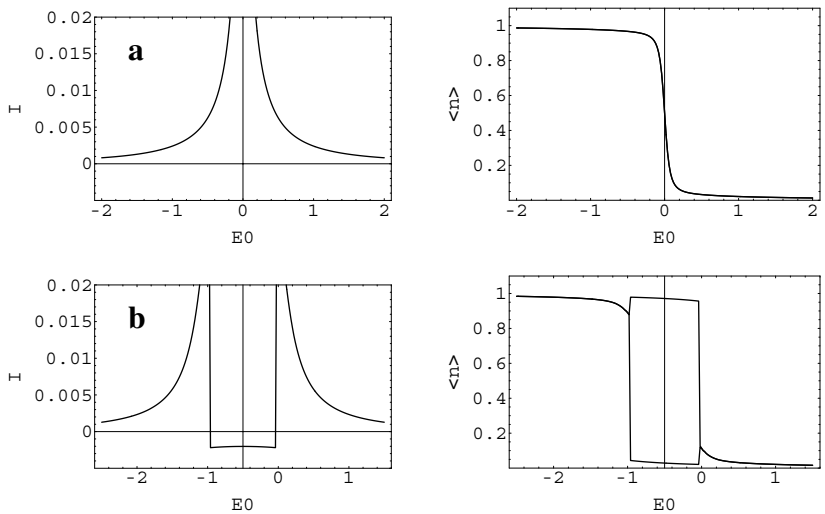

Figure 5. The Josephson current I and the averaged QD occupation number $\langle n_\sigma \rangle$ versus the bare QD level E_0, for (a) QD without interaction and (b) QD with strong interaction. The parameters are: $\Delta = 1$, $\Gamma = 0.1$, $\phi = \pi/2$, $T = 0$, and $U = 0$ for (a) and $U = 1$ for (b).

leading to the supercurrent being always positive with a maximum at $E_0 = -U/2$, and the system behaves in the same way as the non-interacting one. In contrast, if $U > \Gamma$, a symmetry-breaking solution of equation (19) and equation (20) is energy preferred, in which $\langle n_\uparrow \rangle$ and $\langle n_\downarrow \rangle$ are unequal, and the QD becomes a magnetic dot. Consequently, the effective levels $(E'_\uparrow, E'_\downarrow)$ occupy a series of configurations in the negative plane of figure 1, so the Josephson current has a small but negative valley in the I versus E_0 curve. We determine the transition border of the above two cases from the parametric I versus $(-E_0/\Gamma, \Gamma/U)$ diagram shown in figure 6. By virtue of electron–hole symmetry, the diagram is symmetric with respect to $-E_0/U = 0.5$. The black area in figure 6(b) indicates the range of parameters where the S–QD–S system behaves as a π-junction. One can see from the diagram that the system is likely to change to a π-junction around $E_0 = -U/2$.

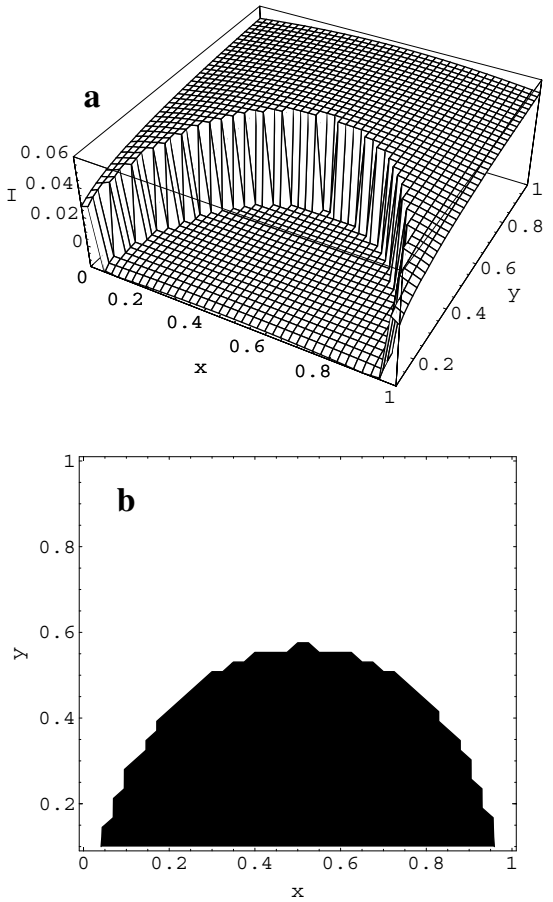

Figure 6. A parametric diagram of the Josephson current I versus parameters $x \equiv -E_0/U$ and $y \equiv \Gamma/U$. We set $\Delta = 1$, $\Gamma = 0.1$, $\phi = \pi/2$, $T = 0$, and change E_0 and U to obtain the surface graph in (a). The black area of (b) indicates the range of parameters where the S–QD–S system behaves as a π-junction.

The temperature dependences are displayed in figure 7, which shows I versus E_0 curves with $U = 1$ for different temperatures. Due to the electron–hole symmetry, only half of the plot is shown. The sharp structure at zero temperature is smoothed at finite temperatures, and

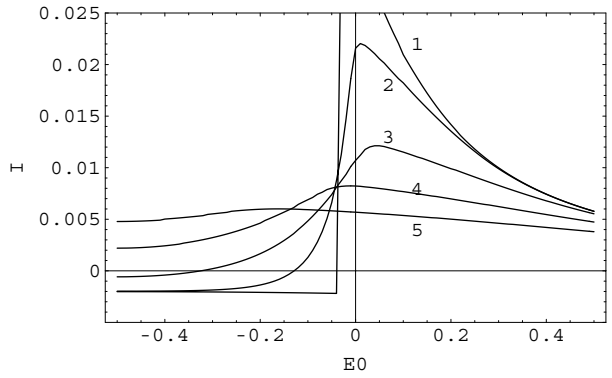

Figure 7. The temperature dependence of I versus E_0. The parameters are: $\Delta = 1$, $\Gamma = 0.1$, $\phi = \pi/2$, $U = 1$; $T = 0.001$, 0.05, 0.10, 0.15, and 0.20 for the curves marked 1, 2, 3, 4, and 5, respectively.

the negative part of the supercurrent vanishes above a critical temperature. These features can be understood by taking account of the temperature effect on the supercurrent through the QD with two spin levels in figure 4 and the temperature effect on the averaged QD occupation numbers. We also studied the diagram of I versus (U, T) where E_0 is set to $-U/2$ (not shown here). The transition line between $I < 0$ and $I > 0$ can be fitted as $U = 0.17 + 7.5T$, which is consistent with the result derived by using the non-crossing approximation in [18].

4. QD in non-equilibrium distribution

Now we turn to discussing the π-junction transition caused by non-equilibrium distribution in the QD. In a recent work by Sun *et al* [24], a mesoscopic four-terminal Josephson junction (S–QD–S with two normal leads connected to the QD) was studied. By using a non-equilibrium Green function method, they found that the supercurrent between the two superconducting electrodes can be suppressed and even reversed by changing the dc voltage applied across the two normal terminals. Here we take the essential point of that work, but omitting its tedious calculation, by simply assuming that the QD has a two-step distribution function:

$$F(\omega) = \frac{1}{2}\left[f(\omega - V_c) + f(\omega + V_c)\right] \xrightarrow{T\to 0} \begin{cases} 1 & \omega < -V_c \\ 0.5 & -V_c < \omega < V_c \\ 0 & \omega > V_c \end{cases} \qquad (22)$$

corresponding to the limit $\Gamma_2 = \Gamma_4 \to 0$ in [24]. Unlike the authors of [24], we allow here the two spin levels of the QD to have a Zeeman splitting, i.e., $E_\uparrow = -E_\downarrow = h$. The curves of the Josephson current $I(\phi = \pi/2)$ versus the control voltage V_c for different Zeeman splittings h are shown in figure 8. These curves are step-like because $F(\omega)$ is step-like at $T = 0$, and $j(\omega)$ has a δ-function-type discrete spectrum in the range $-\Delta < \omega < \Delta$. Either finite temperature or small broadening of the Andreev bound states will smooth the curves.

For $h = 0$, I reverses its sign around $V_c = \Gamma$, and the magnitude of the positive current is much larger than that of the negative one, which is in qualitative agreement with the experiment in [3] and the previous work [24]. For $h \neq 0$, curves of I versus V_c have a peak around $V_c = h$, with a width of about 2Γ, the height being about half of that for $h = 0$. On each side of the peak, there is a negative current valley, where the system behaves as a π-junction. These results are also consistent with the calculations for a non-equilibrium SFS

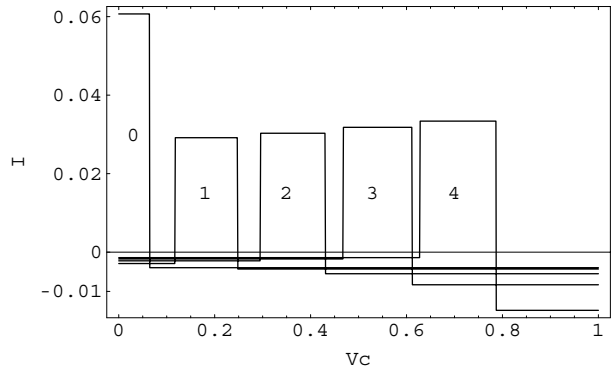

Figure 8. The Josephson current I versus the control voltage V_c for different Zeeman splittings of $E_\uparrow = -E_\downarrow = h$ in the QD. The parameters are: $\Delta = 1$, $\Gamma = 0.1$, $\phi = \pi/2$, $T = 0$; $h = 0$, 0.2, 0.4, 0.6, and 0.8 for the curves marked 0, 1, 2, 3, and 4, respectively.

junction [22, 23]. One can understand these curves by considering the two-step distribution $F(\omega)$ and the CCDOS in figure 4. For example, for the curve for $h = 0.2$ (marked '1' in figure 8), both positive and negative Andreev bound states are above the Fermi surface (see the CCDOS for $(E_\uparrow, E_\downarrow) = (0.2, -0.2)$), located near $h-\Gamma$ and $h+\Gamma$, respectively. When $V_c = h$, the positive bound state has a weight of 0.5, while the negative one has weight 0, reducing the peak height to one half of that for $h = 0$. For both $V_c < h - \Gamma$ and $V_c > h + \Gamma$, the two Andreev bound states have the same weights (either 0 or 0.5), and make little net contribution to the supercurrent. Therefore, the negative continuous spectrum of $\omega < -\Delta$ is dominant in the supercurrent, leading to a π-junction transition on both sides of the positive peak.

5. Conclusions

In this work, we have investigated different mechanisms for the π-junction transition in the S–QD–S system. From the current formula

$$I = 2\sin\phi \int \frac{\mathrm{d}\omega}{2\pi} F(\omega) j(\omega)$$

one can see that the π-junction transition may originate from the change of the CCDOS $j(\omega)$, or the change of the distribution function $F(\omega)$, or from changes of both. The two mechanisms discussed in sections 2 and 3, the Zeeman splitting and intra-dot interaction, are involved the change of the CCDOS $j(\omega)$ only. These two mechanisms are closely connected, since the intra-dot interaction may induce magnetization in the QD if the interaction is strong enough. The third mechanism studied in section 4 involves the change of the distribution function in the QD, and the interplay of the magnetization with the non-equilibrium distribution in the QD. It is interesting that the change of the CCDOS and the change of the distribution have similar effects on the π-junction transition, where the positive and negative Andreev bound states cancel each other, leaving the negative continuous spectrum dominant in the supercurrent. The interplay of the two mechanisms leads to the novel effect that the supercurrent suppressed by magnetization of the QD can be partially recovered if there is an appropriate non-equilibrium distribution of electrons in the QD.

Acknowledgments

This project was supported by the NSFC under grant No 10074001. One of the authors (T-H Lin) would also like to thank the Visiting Scholar Foundation of the State Key Laboratory for Mesoscopic Physics in Peking University for support.

Appendix

In this appendix, we discuss the equation for the Andreev bound states, i.e. $A(\omega) = 0$ with $|\omega| < \Delta$:

$$A(\omega) = \left(\omega - E_\uparrow + \frac{\Gamma\omega}{\sqrt{\Delta^2 - \omega^2}}\right)\left(\omega + E_\downarrow + \frac{\Gamma\omega}{\sqrt{\Delta^2 - \omega^2}}\right) - \frac{\Gamma^2\Delta^2}{\Delta^2 - \omega^2}\cos^2\frac{\phi}{2} = 0. \tag{A.1}$$

Let $\Gamma = \gamma\Delta$, $E_\uparrow = \varepsilon_1\Delta$, $E_\downarrow = -\varepsilon_2\Delta$, $\omega = \Delta\sin\theta$, $\theta \in (-\pi/2, \pi/2)$; the equation now takes a dimensionless form:

$$b(\theta) \equiv (\sin\theta + \gamma\tan\theta - \varepsilon_1)(\sin\theta + \gamma\tan\theta - \varepsilon_2)\cos^2\theta = \gamma^2\cos^2\frac{\phi}{2}. \tag{A.2}$$

Note that the function $y = \sin\theta + \gamma\tan\theta$ projects $\theta \in (-\pi/2, \pi/2)$ monotonically to $y \in (-\infty, +\infty)$. One can find Θ_1 and Θ_2 in $(-\pi/2, \pi/2)$ satisfying

$$\sin\Theta_1 + \gamma\tan\Theta_1 = \varepsilon_1 \qquad \sin\Theta_2 + \gamma\tan\Theta_2 = \varepsilon_2.$$

Suppose $\Theta_1 < \Theta_2$; we have $b(\theta) \geqslant 0$ for $\theta \in (-\pi/2, \Theta_1] \cup [\Theta_2, \pi/2)$, and $b(\theta) < 0$ for $\theta \in (\Theta_1, \Theta_2)$. Because $b(\pm\pi/2) = \gamma^2$, equation (A.2) has at least two roots, $\theta_1 \in (-\pi/2, \Theta_1]$ and $\theta_2 \in [\Theta_2, \pi/2)$ for $\phi \neq 0$. It is straightforward to find the two roots by the dichotomy method.

Next, we prove that $b'(\theta) \geqslant 0$ for $0 < b(\theta) < \gamma^2$ and $\theta \in [\Theta_2, \pi/2)$, while $b'(\theta) \leqslant 0$ for $0 < b(\theta) < \gamma^2$ and $\theta \in (-\pi/2, \Theta_1]$, which means that θ_1 and θ_2 are the only two roots in $(-\pi/2, \Theta_1]$ and $[\Theta_2, \pi/2)$. For $\theta \in [\Theta_2, \pi/2)$, $\sin\theta + \gamma\tan\theta - \varepsilon_1 \geqslant 0$ and $\sin\theta + \gamma\tan\theta - \varepsilon_2 \geqslant 0$. Define $x \equiv [(\sin\theta + \gamma\tan\theta - \varepsilon_1)(\sin\theta + \gamma\tan\theta - \varepsilon_2)]^{1/2}$. Because $0 < b(\theta) < \gamma^2$, one obviously has $0 < x < \gamma\sec\theta$, and

$$\begin{aligned} b'(\theta) &= 2\left(\sin\theta + \gamma\tan\theta - \frac{\varepsilon_1 + \varepsilon_2}{2}\right)(\gamma + \cos^3\theta) \\ &\quad - 2\sin\theta\cos\theta(\sin\theta + \gamma\tan\theta - \varepsilon_1)(\sin\theta + \gamma\tan\theta - \varepsilon_2) \\ &\geqslant 2x\gamma - 2(\cos\theta)x^2 = -2(\cos\theta)x(x - \gamma\sec\theta) \geqslant 0. \end{aligned} \tag{A.3}$$

Therefore, equation (A.2) has, and only has, two roots in the range $\theta \in (-\pi/2, \pi/2)$ for $\phi \neq 0$.

For $\phi = 0$, because $b'(\pi/2) = -2\gamma[2 - (\varepsilon_1 + \varepsilon_2)]$, $b'(-\pi/2) = 2\gamma[2 + (\varepsilon_1 + \varepsilon_2)]$, and considering the properties of $b'(\theta)$, one can clearly see that equation (A.2) has two roots in $(-\pi/2, \pi/2)$ if $|\varepsilon_1 + \varepsilon_2| < 2$, but only has one root in $(-\pi/2, \pi/2)$ if $|\varepsilon_1 + \varepsilon_2| \geqslant 2$. However, this case is irrelevant to the Josephson effect.

References

[1] Morpurgo A F, Klapwijk T M and van Wees B J 1999 *Appl. Phys. Lett.* **72** 966
[2] Kutchinsky J, Taboryski R, Sørensen C B, Hansen J B and Lindelof P E 1999 *Phys. Rev. Lett.* **83** 4856
[3] Baselmans J J, Morpurgo A F, Klapwijk T M and van Wees B J 1999 *Nature* **43** 397
[4] Nakano H and Takayanagi H 1993 *Phys. Rev.* B **47** 7986
[5] Ilhan H T, Demir H V and Bagwell P F 1998 *Phys. Rev.* B **58** 15 120
[6] Blonder G E, Tinkham M and Klapwijk T M 1982 *Phys. Rev.* B **25** 4515

[7] van Wees B J, Lenssen K-M H and Harmans C J P M 1991 *Phys. Rev.* B **44** 470
[8] Wendin G and Shumeiko V S 1996 *Phys. Rev.* B **53** R6006
[9] Chang L-F and Bagwell P F 1997 *Phys. Rev.* B **55** 12 678
[10] Wendin G and Shumeiko V S 1996 *Superlatt. Microstruct.* **20** 569
[11] Samuelsson P, Shumeiko V S and Wendin G 1997 *Phys. Rev.* B **56** R5763
[12] Volkov A F 1995 *Phys. Rev. Lett.* **74** 4730
[13] Volkov A F and Takayanagi H 1997 *Phys. Rev.* B **56** 11 184
[14] Yip S-K 1998 *Phys. Rev.* B **58** 5803
[15] Wilhelm F K, Schön G and Zaikin A D 1998 *Phys. Rev. Lett.* **81** 1682
[16] Glazman L I and Matveev K A 1989 *JETP Lett.* **49** 659
[17] Spivak B I and Kivelson S A 1991 *Phys. Rev.* B **43** 3740
[18] Ishizaka S, Sone J and Ando T 1995 *Phys. Rev.* B **52** 8358
[19] Rozhkov A V and Arovas D P 1999 *Phys. Rev. Lett.* **82** 2788
[20] Clerk A A and Ambegaokar V 1999 *Preprint* cond-mat/9910201
[21] Prokić V, Buzdin A I and Dobrosavljević-Grujić L 1999 *Phys. Rev.* B **59** 587
[22] Yip S-K 2000 *Phys. Rev.* B **62** R6127
[23] Heikkilä T T, Wilhelm F K and Schön G 2000 *Preprint* cond-mat/0003383
[24] Sun Q-F, Wang J and Lin T-H 2000 *Phys. Rev.* B **62** 648
[25] Sun Q-F, Wang B-G, Wang Jian and Lin T-H 2000 *Phys. Rev.* B **61** 4754
[26] Furusaki A and Tsukada M 1990 *Physica* B **165+166** 967
[27] Beenakker C W J and van Houten H 1991 *Phys. Rev. Lett.* **66** 3056
[28] Bagwell P F 1992 *Phys. Rev.* B **46** 12 573
[29] Anderson P W 1961 *Phys. Rev.* **124** 41